Calculation of Fully Developed Flow and Heat Transfer in Streamwise-Periodic Dimpled Channels

Dipankar Choudhury*
Creare Inc., Hanover, New Hampshire 03755
and
Kailash C. Karki†
University of Minnesota, Minneapolis, Minnesota 55455

An analysis is presented for fluid flow and heat transfer in a parallel plate channel with periodically spaced dimples. The flow is assumed to be constant property, two dimensional and laminar, with uniform wall temperature thermal boundary condition in the periodic fully developed region. A control-volume finite-difference method based on generalized curvilinear coordinates with the capability to handle periodic boundary conditions has been developed in order to solve the problem. Computations have been carried out for a variety of geometric parameter, Reynolds number, and Prandtl number combinations. Local results presented for the periodic fully developed velocity and temperature fields provide a good physical understanding of the fluid flow and heat transfer phenomena. The average heat transfer and pressure drop results are presented for all the cases studied. Decrease in the channel width and the dimple spacing are both accompanied by increase in the heat transfer and pressure drop.

Nomenclature

B = overall pressure gradient, Eq. (1)
C_p = specific heat of fluid at constant pressure
D = dimple diameter, Fig. 1
D_H = hydraulic diameter of the channel, Eq. (10)
f = Darcy friction factor, Eq. (11)
H = height of the dimple, Fig. 1
h = local heat transfer coefficient on upper and lower walls, Eq. (22)
$\bar{h}$ = average heat transfer coefficient based on parallel plate channel area, Eq. (19)
k = thermal conductivity of the fluid
L = separation between dimples, Fig. 1
$LMTD$ = log-mean temperature difference for the module, Eq. (20)
Nu = local Nusselt number for the module, Eq. (21)
$\overline{Nu}$ = average Nusselt number for the module, Eq. (18)
Nu_0 = fully developed Nusselt number for a parallel plate channel
P = periodic part of static pressure, Eq. (1)
p = static pressure
Pr = Prandtl number of the fluid, Eq. (17)
Q = per-module heat transfer rate
q = local heat flux over the channel surface
Re = Reynolds number, Eq. (8)
T = temperature
T_b = bulk temperature of the fluid, Eq. (14)
T_w = uniform temperature of the channel walls
u,v = Cartesian velocity components
$\bar{u}$ = average velocity of the fluid in x direction, Eq. (9)
x,y = Cartesian coordinates
Γ = diffusion coefficient
ϕ = general dependent variable
ξ,η = curvilinear coordinates
μ = dynamic viscosity of the fluid
ρ = density of the fluid
θ = dimensionless temperature, Eq. (13)
Ψ_0 = maximum value of normalized stream function in the main recirculating eddy

Subscripts

b = bulk value
w = value at channel wall
0 = parallel plate channel value

Received Jan. 27, 1989; revision received Aug. 12, 1989.

*Engineer, Computational Fluid Dynamics. Member AIAA.
†Research Associate, Department of Mechanical Engineering. Member AIAA.

Introduction

THE phenomenon of streamwise-periodic fluid flow and heat transfer is encountered in a variety of situations, such as flow in compact heat exchanger channels and flow across tube banks. Applications such as the cooling of avionics components, computer circuit boards in supercomputers, and radiators in the aerospace and automobile industries require compact and efficient heat exchange devices. The flow passages in these devices are usually characterized by small dimensions and low velocities, and, therefore, the flow is laminar for a significant fraction of the range of operation. Since heat transfer coefficients in laminar flow are generally low for smooth channels, a variety of unconventional internal flow passage designs is used to augment the heat transfer rates. Examples of these passages occur in corrugated wall ducts, channels with wavy walls, parallel plate channels with staggered fins, and plate-fin heat exchangers.

In many of the duct configurations mentioned above, the geometry varies in a periodic manner along the direction of the flow. The concept of a periodic fully developed regime, described by Patankar et al.,[1] can be used in the analysis of these periodic geometries, since the flow pattern repeats itself in successive cycles downstream of an entrance region. The onset of the periodic fully developed regime occurs, in practice, about five hydraulic diameters downstream of the duct inlet.[2] In typical applications, where the flow passage consists of many modules, the concept of the periodic fully developed regime is a reasonable model. When the thermal boundary conditions are of a particular type, such as uniform wall temperature or uniform constant wall heat flux, the temperature field (when scaled in an appropriate manner) also becomes periodically fully developed, as shown in Ref. 1. Thus, the entire analysis of fluid flow and heat transfer can be restricted to one module of the duct with a resultant economy of computational effort.

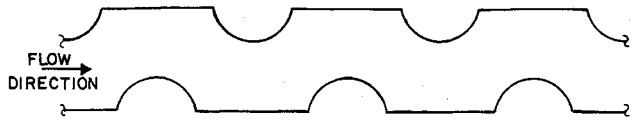

Fig. 1a The dimpled channel geometry.

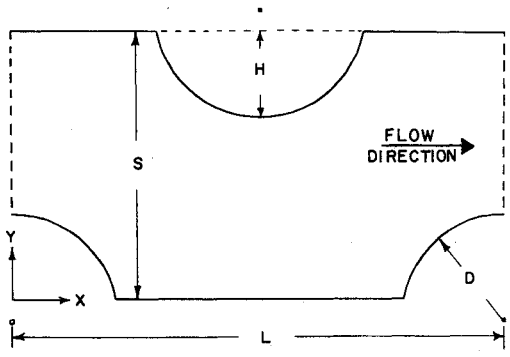

Fig. 1b The domain in physical coordinates.

The purpose of this paper is to analyze the flow and heat transfer in a particular geometry that belongs to the class of streamwise-periodic geometries described in the previous paragraphs. The geometry, shown in Fig. 1a, consists of a parallel plate channel with semicircular dimples arranged in a staggered manner along the upper and lower walls. This duct configuration is used, among other places, to enhance heat transfer performance of radiator cooling passages. It appears that no experimental or numerical results are available in the literature for dimpled channel ducts despite their importance, and this provides the motivation for the present work. The dimples serve to provide additional surface area for heat transfer as well as improve the heat transfer performance by causing flow deflection and impingement on the upper and lower walls of the channel. The details of the geometry are shown in Fig. 1b, where it can be seen that the dimples have the same height H, which provides a partial blockage of the flow area between the upper and lower plates separated by a distance S. The dimples are arranged at a regular interval of length L, which defines the length of the computational domain. As indicated by Kelkar and Patankar[3] in a study of fluid flow and heat transfer in parallel plate channels with staggered fins, the geometric parameters and the arrangement of the dimples have the potential of having a tremendous effect on the pressure drops and heat transfer performance of the duct.

In this work, in order to properly model the dimpled channel geometry, the generalized curvilinear coordinate finite-volume method of Karki and Patankar[4] has been extended to handle streamwise-periodic problems. Due to the shape of the boundaries of the present problem, usual methods based on simple orthogonal meshes, such as Cartesian grids, cannot be used. In the present method, a nonorthogonal grid based on curvilinear coordinates is generated in the domain, such that the boundaries conform to coordinate lines. The governing transport equations are then solved in the numerically generated mesh, using a control-volume finite-difference method. Although curvilinear coordinate methods, as applied to streamwise-periodic problems, have been reported in the literature (for example, Asako and Faghri[5] and Garg[6]), the techniques used in these papers are based on specific algebraic transformations that transform the physical domain to a rectangle. Algebraic transformation methods, although simple to implement, are special cases of the general boundary-fitted coordinate methods and, as such, are limited to specific geometries. The present method, however, is not limited to particular boundary shapes, and very complex geometries can be modeled.

In this paper, a numerical analysis of the dimpled channel problem is presented, together with detailed local and overall results for fluid flow and heat transfer. The flow is assumed to be steady, two dimensional, and laminar. The thermal boundary condition along the duct walls is that of uniform wall temperature. The calculations have been carried out for three values of the dimensionless channel width and dimple spacing, encompassing a Reynolds number range between 100 and 1000. The heat transfer results have been obtained for two values of the Prandtl number of 0.7 and 5. Although the present analysis does not account for vortex shedding that may occur at high Reynolds number for some of the configurations, it is felt that the effect of vortex shedding (assuming it is present) would be to further increase the heat transfer rate and pressure drop. The results reported here can, therefore, be considered to be conservative. Calculations with unsteady equations would yield marginally more useful information at the expense of excessive computational costs.

Mathematical Formulation

As mentioned previously, since the geometry shown in Fig. 1a has a repetitive pattern in the streamwise direction, the calculation can be restricted to a typical module, shown in Fig. 1b. The concept of a periodic fully developed flow regime and a calculation procedure that takes advantage of this phenomenon, have been described by Patankar et al.[1] and, therefore, the description here will be limited to the important features and the details related to the employment of curvilinear coordinates. In streamwise-periodic ducts, such as the dimpled channel problem described here, the velocity field repeats itself at corresponding axial locations in the modules in the streamwise direction. In addition, the pressure at these cyclic locations decreases linearly downstream. When thermal boundary conditions, such as uniform wall heat flux or uniform wall temperature are imposed, a periodic thermally developed regime develops that is characterized by a module averaged heat transfer coefficient that is the same from module to module.

Conservation Equations in Cartesian Coordinates

As explained in Ref. 1, the pressure p in a periodic fully developed flow can be expressed as a linear combination of an overall pressure drop (which drives the flow in the streamwise direction) and a "local" pressure P that is responsible for local flowfield variations in the module:

$$p(x,y) = -Bx + P(x,y) \tag{1}$$

where B is a constant representing the overall pressure gradient. Thus, BL is the pressure drop in a given module. The "local" pressure $P(x,y)$ behaves in a periodic manner from module to module, such that

$$P(x,y) = P(x + L,y) \tag{2}$$

The governing equations of continuity and momentum have the following form for incompressible constant property flow:

$$\frac{\partial u}{\partial x} + \frac{\partial v}{\partial y} = 0 \tag{3}$$

$$\rho\left(u\frac{\partial u}{\partial x} + v\frac{\partial u}{\partial y}\right) = B - \frac{\partial P}{\partial x} + \mu\left(\frac{\partial^2 u}{\partial x^2} + \frac{\partial^2 u}{\partial y^2}\right) \tag{4}$$

$$\rho\left(u\frac{\partial v}{\partial x} + v\frac{\partial v}{\partial y}\right) = -\frac{\partial P}{\partial y} + \mu\left(\frac{\partial^2 v}{\partial x^2} + \frac{\partial^2 v}{\partial y^2}\right) \tag{5}$$

The appropriate boundary conditions along the upper and lower walls and the periodic boundaries ($x = 0$ and $x = L$) are

$$\text{Wall surface: } u = 0, \qquad v = 0 \tag{6}$$

$$x = 0, \qquad x = L: u(0,y) = u(L,y)$$

$$v(0,y) = v(L,y) \tag{7}$$

It may be noted that due to the nature of the periodic boundary conditions, no inflow velocities are specified. However, the value of B determines the flow rate through the channel. On examining the fluid flow equations and the geometry, the fluid flow is governed by the geometrical parameters H/S and L/S and the Reynolds number, defined as

$$Re = \rho \bar{u} D_H / \mu \tag{8}$$

where

$$\bar{u} = \frac{1}{S}\int_0^S u \, dy \tag{9}$$

$$D_H = 2S \tag{10}$$

The friction factor is defined in the usual manner:

$$f = BD_H/(\tfrac{1}{2}\rho \bar{u}^2) \tag{11}$$

With the Reynolds number Re, hydraulic diameter D_H, and the friction factor f defined as above, direct comparisons are possible with the friction factor corresponding to a parallel plate channel.

The governing equation for the temperature field is

$$\rho C_p\left(u\frac{\partial T}{\partial x} + v\frac{\partial T}{\partial y}\right) = \frac{\partial}{\partial x}\left(k\frac{\partial T}{\partial x}\right) + \frac{\partial}{\partial y}\left(k\frac{\partial T}{\partial y}\right) \tag{12}$$

With the thermal boundary condition of specified uniform wall temperature T_w on the upper and lower walls, the dimensionless temperature field becomes periodic. The dimensionless temperature θ is defined as

$$\theta = \frac{T - T_w}{T_b - T_w} \tag{13}$$

and repeats from module to module. The bulk temperature T_b in Eq. (13) is given by

$$T_b = \int_0^S |u| T \, dy \Big/ \int_0^S |u| \, dy \tag{14}$$

as is appropriate for recirculating flows. The boundary conditions for temperature are as follows:

$$\text{Wall surface: } \theta = 0 \tag{15}$$

$$x = 0, \quad x = L: \ \theta(0,y) = \theta(L,y) \tag{16}$$

The solution of the heat transfer problem introduces an additional parameter, the Prandtl number, defined as

$$Pr = C_p \mu / k \tag{17}$$

The overall heat transfer performance of the dimpled channel can be measured by the average Nusselt number, given by

$$\overline{Nu} = \bar{h} D_H / k \tag{18}$$

where the average convective heat transfer coefficient is defined, such that

$$\bar{h} = Q/(2L)(LMTD) \tag{19}$$

with Q being the total rate of heat transfer in the module. The definition of $\bar{h}$ in Eq. (19) is based on a surface area of $2L$, which is the surface area of a parallel plate channel of the same length. Thus, the extra area due to the curvature of the dimpled surface is not taken into account. The quantity $LMTD$ in Eq. (19) represents the log-mean temperature difference, defined as

$$LMTD = \frac{[T_w - T_b(L)] - [T_w - T_b(0)]}{\ln\{[T_w - T_b(L)]/[T_w - T_b(0)]\}} \tag{20}$$

A local Nusselt number is also computed for the upper and lower walls of the channel as

$$Nu = hD_H/k \tag{21}$$

where

$$h = q/(T_w - T_b) \tag{22}$$

Computational Procedure for Flow and Heat Transfer in Generalized Coordinates

In the present paper, the calculation procedure of Refs. 4 and 7 has been used to solve the conservation equations in generalized curvilinear coordinates. In this section, important features of the method are presented; complete details can be found in the above cited references.

The calculation procedure is based on the finite-volume formulation,[8] in which the physical domain is divided into contiguous control volumes. A staggered grid arrangement is used in which the scalar quantities are located at the center of a control volume and the velocity components are displaced along the coordinate directions to lie at the midpoints of the control-volume faces. The momentum equations are written in terms of the physical covariant (grid-oriented) velocity components. Due to the spatial variation of the base vectors associated with these velocity components, curvature source terms appear in the governing equations. In the method proposed in Refs. 4 and 7, a locally fixed coordinate system is used to derive the discretization equations for the curvilinear velocity components. In this approach, the coordinate axis, in the direction of the velocity component being considered, is fixed at the neighboring points. Thus, all velocity components appearing in the discretization equation are parallel, and curvature terms do not appear explicitly in the formulation. This procedure is only slightly more complex than that for a simple coordinate system. The coupling between the velocity and pressure fields is handled using the SIMPLER algorithm.[8] The calculation procedure has been used to solve a variety of benchmark problems, and the results are documented in Refs. 4 and 7.

In the present work, the solution method was modified to incorporate the features related to the streamwise periodicity of the flow. A cyclic tri-diagonal matrix algorithm (TDMA) was implemented to solve the discretization equations. To enhance the convergence of the cyclic TDMA, the additive correction method of Settari and Aziz[9] was incorporated. The solution of the flowfield for a desired value of the Reynolds number was accomplished by starting the calculation procedure with an arbitrary value of B and a tentative value of the viscosity μ. With these values specified, the calculation yielded an average velocity $\bar{u}$ that was used to adjust μ to give the desired value of Re. The iterative updating of μ was continued until convergence. The solution of the temperature field presented some additional difficulties, because Eq. (12) and the boundary conditions of Eqs. (15) and (16) constitute an eigenvalue problem with the θ field being periodic and not T, so that the bulk temperature $T_b(x)$ is not known a priori at any streamwise location. Kelkar and Patankar[3] have suggested an iterative procedure that addresses this problem, and a similar procedure extended to curvilinear coordinates is used in this work.

The computations were performed on a 42×42 numerically generated grid using a differential equations method described by Thompson et al.[10] With the boundary grid point distribution being specified in the (x,y) coordinate system, the solution to a set of Poisson equations constitutes a boundary value problem whose result is the grid point distribution in the

interior of the domain. The grid points in the η and ξ (curvilinear coordinates) directions were distributed in a nonuniform manner, with a higher concentration of grid lines close to the walls, as shown in Fig. 2. Some amount of grid control using attraction functions, described in Ref. 10, was necessary in order to prevent migration of grid lines. Additional runs for coarser (32×32) and finer (52×52 and 62×62) meshes and meshes with different grid point distributions indicated that the reported values of $\overline{Nu}$ and f are within 3% of the extrapolated values for a grid with an infinite number of grid points.

In all the computations involved in this study, calculation of the temperature field was started only after a converged velocity field was obtained. The velocity field was deemed to be converged when the maximum value of the normalized mass residual was less than 10^{-5}, and the temperature field was taken to be converged when the heat balance in the module was within 10^{-4}%. Typical computations required about 250 iterations for a converged velocity field and about 40 additional iterations for a converged temperature field corresponding to each Prandtl number. The computer program used for the computations was optimized to run efficiently on an Alliant FX/8 minisupercomputer, with a large fraction of the code being able to utilize the vectorization capability of this machine. Typical run times on a single processor was of the order of 20 CPU minutes. Expected run times on a CRAY-1S supercomputer are about 2 CPU minutes.

Results and Discussion

The computer code has been tested on a variety of benchmark problems, and the results have been documented in Refs. 4 and 7. In particular, the periodic boundary condition capability developed in this work has been validated by solving fully developed channel flow problems, for which the exact solutions are known, with periodic boundary conditions. The results of the code are in excellent agreement with the closed form solutions for both velocity and temperature fields. In addition, the forced convection problem in two corrugated duct geometries has been solved with the computer program developed in this work. For the first problem, the predicted average Nusselt number (using an 82×32 grid) has been compared with the experimental results of Goldstein and Sparrow[11] for an isothermal corrugated duct, with $Re = 510$ and $Pr = 0.6354$. The experimental and predicted Nusselt numbers are 8.6 and 9.09, respectively—a difference of about 6%. In the second series of test problems, some selected corrugated duct geometries studied by Asako and Faghri[5] were modeled for a range of Reynolds and Prandtl numbers. The results for the friction factor f and the average Nusselt number $\overline{Nu}$ were within 5% of the published results.

The results of primary interest in this study were the module-averaged heat transfer and the friction factor coefficients. When the important dimensions of the geometry are scaled with the spacing between the upper and lower walls, S, the fluid flow and heat transfer results become functions of two geometrical parameters (L/S and H/S), the Reynolds number, and the Prandtl number. The influence of these parameters was studied by choosing three values of L/S (1.875, 2.5, and 3.2), three values of H/S (0.25, 0.32, and 0.4), four values of the Reynolds number (100, 200, 500, and 1000) and two values of the Prandtl number (0.7 for air and 5 for water). The choice of the values of the geometrical parameters was dictated by manufacturing constraints in the sheet metal forming process used to manufacture the dimpled channels. For example, the dimples cannot be made too high (the height is limited to 0.4 diam) nor can the spacing between the dimples be too small (L/S is restricted to a minimum value of 1.875). Calculations were not performed for Reynolds number greater than 1000 because the flow is unlikely to remain laminar for values that are appreciably greater.

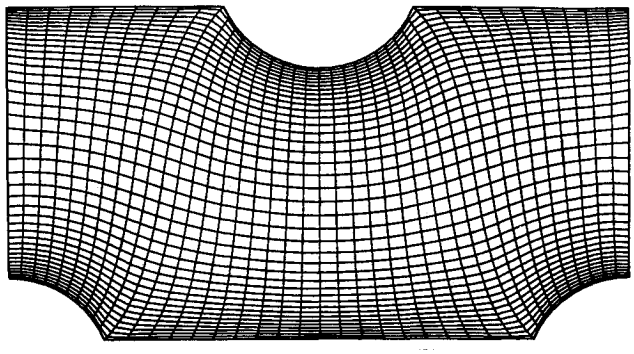

Fig. 2 A typical grid distribution for the geometry considered.

Flow Patterns and Isotherm Maps

Representative results for the flowfield are shown via vector plots in Figs. 3a and 3b. These figures are for $H/S = 0.4$, $L/S = 1.875$, $Re = 100$, and $Re = 1000$, respectively. As seen in the figures, the presence of the relatively tall dimples relative to the module length causes considerable flow distortion. The flow negotiates the peaks and valleys in the domain in an undulating fashion that causes considerable impingement. For $Re = 100$, there is very little flow separation downstream of the dimples, and the gradients at the walls are not as steep as in the $Re = 1000$ case. In Fig. 3b, for $Re = 1000$, the separated region has become much larger, with a large recirculation region occupying the entire space between two successive dimples. The high velocity core flow impinges on the upstream side of the dimples with sharp gradients and, therefore, these zones are expected to be very active in heat transfer. Also, the straight walls are seen to be adjacent to the lower velocity recirculation zones, so that lower heat transfer coefficients are expected on these walls. Both Figs. 3a and 3b clearly indicate the periodic nature of the velocity field, which, incidentally, also exhibits an antisymmetry due to the equally spaced staggered arrangement of the dimples.

The streamline plots in Figs. 4–6 show the effect of different parameters on the flowfield. The effect of the Reynolds number is shown in Fig. 4 for fixed values of $H/S = 0.32$ and

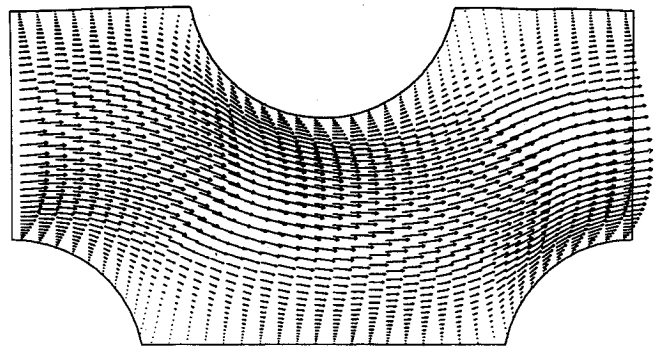

a) $Re = 100$

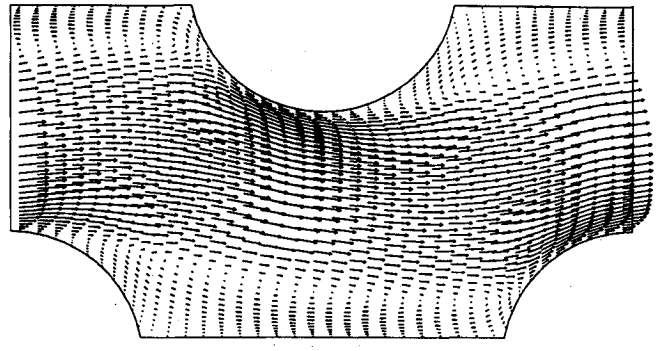

b) $Re = 1000$

Fig. 3 Velocity field for $H/S = 0.32$, $L/S = 1.875$.

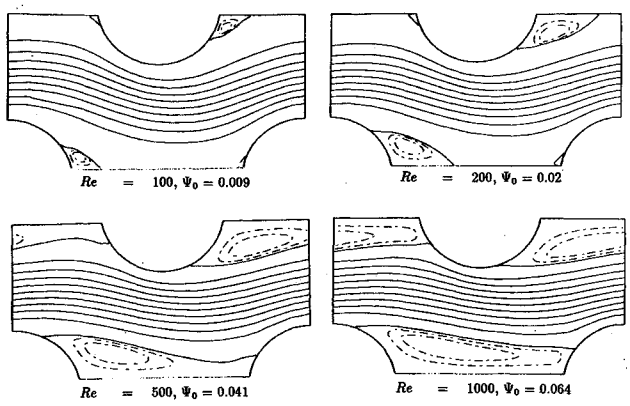

Fig. 4 Streamline plots for $H/S = 0.32$, $L/S = 1.875$, and varying Re.

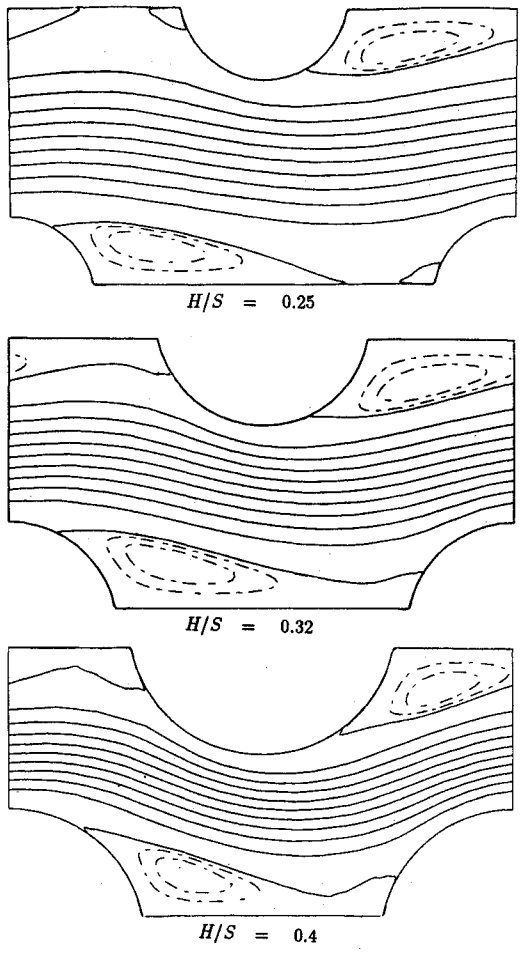

Fig. 5 Streamline plots for $L/S = 1.875$, $Re = 500$, and varying H/S.

$L/S = 1.875$. As Re increases, or, in other words, as the flow rate increases through the channel, the size and the strength of the recirculation zone grows. For $Re = 100$ and $Re = 200$, very small secondary recirculation bubbles can be seen upstream of the dimples at the junctions of the straight and curved walls. However, at larger values of Re, the primary and secondary eddies join to form large eddies that occupy the entire interdimple space. The strength of the recirculating flow in each case can be judged from the value of the maximum dimensionless streamfunction Ψ_0, which can also be interpreted as the ratio of the flow in the recirculation zone to the flow rate of the throughflow.

The effect of increasing the H/S ratio for $L/S = 1.875$ and $Re = 500$, which is equivalent to decreasing the spacing between the upper and lower walls of the channel or increasing

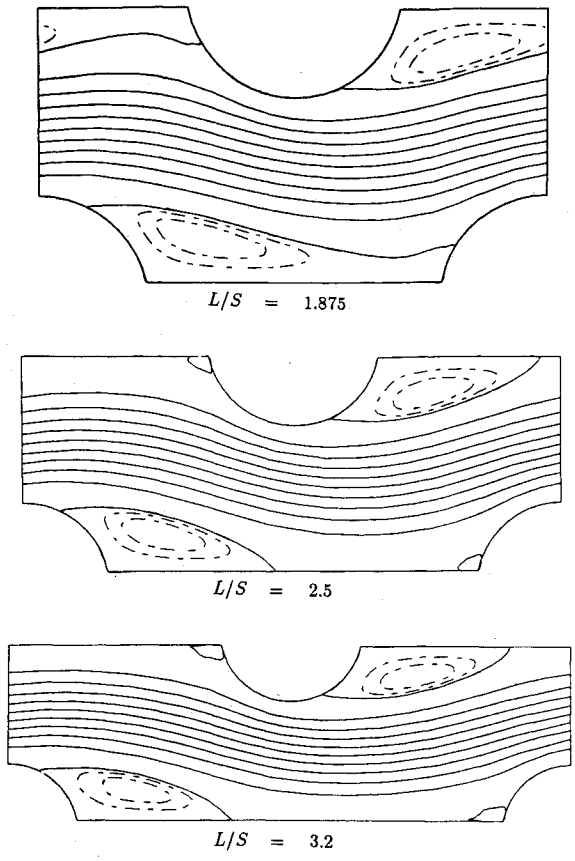

Fig. 6 Streamline plots for $H/S = 0.32$, $Re = 500$, and varying L/S.

the dimple height relative to the spacing, is shown in Fig. 5. As H/S increases, the throughflow is constricted and bends more significantly with the distortion in the streamlines becoming more and more severe. It is apparent that the presence of taller dimples causes more flow impingement on the upstream side of the dimples. The streamline maps in Fig. 6 show the effect of increasing the L/S ratio (the module length relative to the channel spacing), keeping H/S and Re fixed at 0.32 and 500, respectively. The effect of decreasing the dimple spacing is qualitatively quite similar to that of increasing the Reynolds number.

Figure 7 shows the effect of Reynolds number and the Prandtl number on the temperature field for a typical geometry ($H/S = 0.32$, $L/S = 1.875$). It should be noted that the isotherms correspond to the dimensional temperature T, and not θ, so that the plots are physically more meaningful. The contour plots of θ show a periodic behavior unlike the developing pattern for the dimensional temperature observed in Fig. 7. It is apparent from the spacing of the isotherms that at a given value of Re, the temperature field for $Pr = 5.0$ is characterized by thinner boundary layers, compared to the $Pr = 0.7$ case, due to lesser thermal diffusion effects. Thus, higher heat transfer coefficients are expected for larger values of the Prandtl number. Another observation that is readily made is that the thermal boundary layer is thinner at higher Reynolds numbers. At higher flow rates, the core flow tends to cool down, or heat up as the case may be, at a slower rate. Thinner boundary layers imply higher heat transfer coefficients. The plot corresponding to $Re = 500$ and $Pr = 5$ clearly shows the impingement effects of the core flow on the upstream side of the dimple, where the isotherms are seen to be very closely packed together. Temperature gradients in these regions are high and, as will be shown later in this paper, the local heat transfer coefficients are also high. Also, the effect of the strong recirculating flow is more apparent at $Pr = 5$ than at $Pr = 0.7$, as shown by the kinks in some of the isotherms.

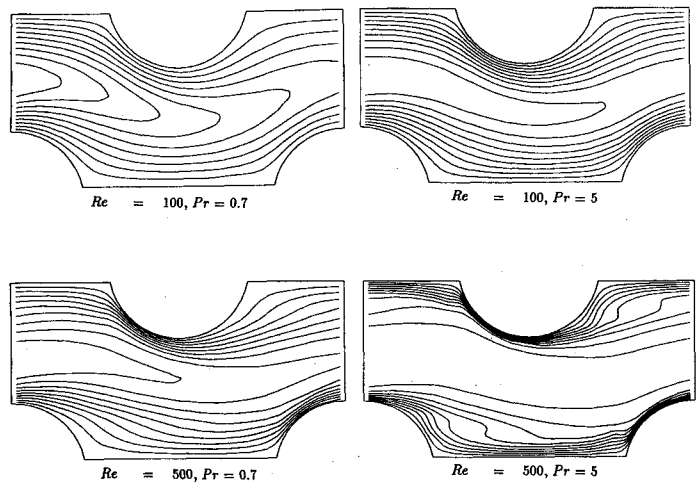

Fig. 7 Isotherm plots for $H/S = 0.32$, $L/S = 1.875$, and varying Re and Pr.

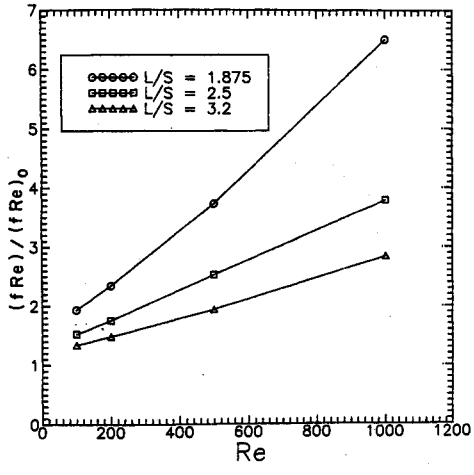

Fig. 8 Influence of Re and L/S on fRe for $H/S = 0.25$.

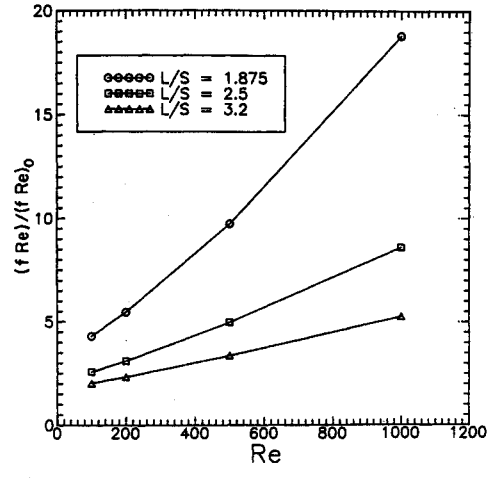

Fig. 10 Influence of Re and L/S on fRe for $H/S = 0.4$.

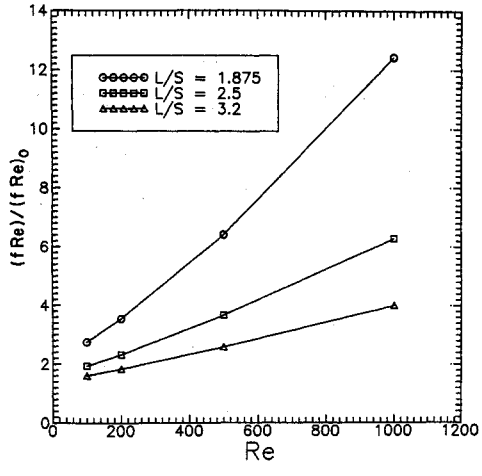

Fig. 9 Influence of Re and L/S on fRe for $H/S = 0.32$.

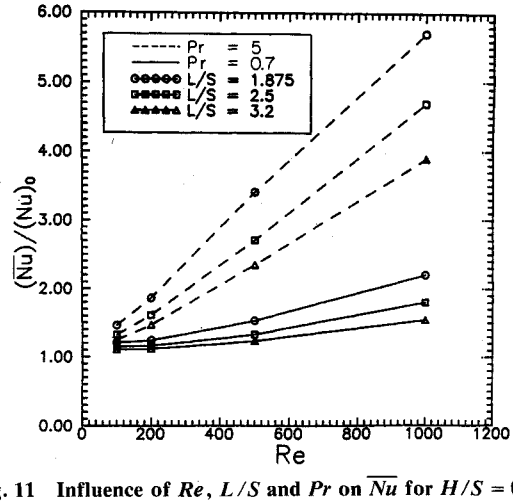

Fig. 11 Influence of Re, L/S and Pr on $\overline{Nu}$ for $H/S = 0.25$.

Friction Factor and Average Nusselt Number

In the interest of clarity, the friction factor and average Nusselt numbers for all the cases studied have been presented as a function of the Reynolds number in six different figures (Figs. 8–13). In these figures, the results have been presented in terms of the ratios $fRe/(fRe)_0$ and $\overline{Nu}/\overline{Nu}_0$, where $(fRe)_0$ and $\overline{Nu}_0$ represent values corresponding to a parallel plate channel with isothermal walls. These values are $(fRe)_0 = 96$ and $\overline{Nu}_0 = 7.54$; ratios greater than unity indicate pressure drop penalty and heat transfer augmentation relative to a parallel plate channel without dimples. Each pair of friction factor and average Nusselt number plots corresponds to a given value of the H/S ratio (0.25, 0.32, and 0.4). On each plot, the L/S ratio is used as a parameter with values of 1.875, 2.5, and 3.2. The Nusselt number plots display two sets of curves corresponding to $Pr = 0.7$ and $Pr = 5$.

In all the cases, both fRe and $\overline{Nu}$ increase uniformly with Reynolds number. The increase in heat transfer with Reynolds number is directly linked to the flow impingement effects at higher flow rates. The increasing flow separation and impingement also introduce a pressure drop penalty, however. The

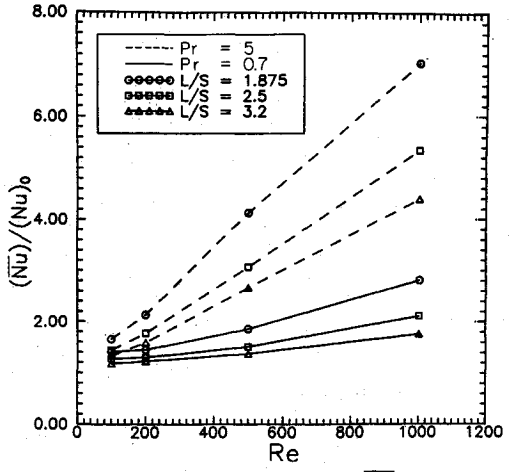

Fig. 12 Influence of Re, L/S and Pr on $\overline{Nu}$ for $H/S = 0.32$.

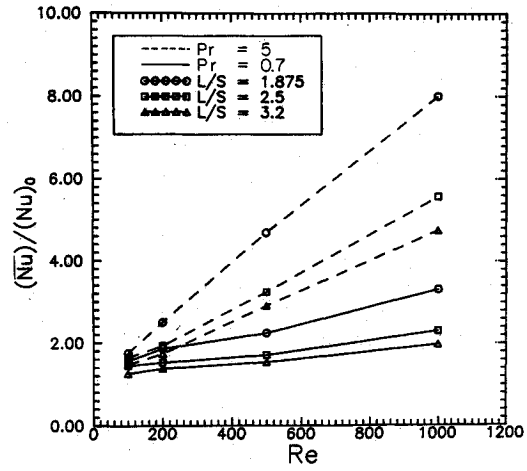

Fig. 13 Influence of Re, L/S and Pr on $\overline{Nu}$ for $H/S = 0.4$.

heat transfer rate is observed to be significantly higher for the larger value of the Prandtl number. Although, in the best case ($Re = 1000$, $H/S = 0.4$, $L/S = 1.875$, and $Pr = 5.0$) the heat transfer rate is augmented by as much as a factor of eight, the pressure drop penalty is even higher with the $fRe/(fRe)_0$ ratio being about 18.

The effect of increasing L/S can be seen in each plot, where both fRe and $\overline{Nu}$ decrease with an increase in L/S at fixed values of Re and H/S. As observed earlier, the flowfield is less distorted when the dimple spacing is increased. Thus, as the dimple spacing gets larger, the friction factor and Nusselt number behavior approaches that of a parallel plate channel without dimples. The heat transfer behavior is consistent with the fact that with increasing distance between dimples there is less frequent breakup of the thermal boundary layer.

The effect of increasing the ratio H/S can be seen by comparing the three sets of friction factor and Nusselt number plots. The friction factor ratio is seen to rise rather rapidly with increase in the H/S ratio, whereas the Nusselt number ratio rises at a lesser rate. As the spacing is decreased or the dimple height is increased, for a given flow rate, the average velocity increases linearly, but the associated pressure drop increases approximately as the square of this velocity. With increasing H/S, the recirculation regions downstream of the dimple, which do not contribute much to the heat transfer, become larger and larger and the gain in heat transfer performance suffers. Therefore, it appears that even if manufacturing constraints are not considered, there may not be much to gain by going to very tall dimples or small channel spacings.

Local Heat Transfer

Figure 14 shows the variation of the local Nusselt number Nu on the upper and lower surfaces of the channel along the streamwise coordinate x. The local Nusselt number has been scaled with $\overline{Nu}_0$, and the streamwise coordinate has been nondimensionalized with the module length L. The plot corresponds to $H/S = 0.32$, $L/S = 1.875$, and $Pr = 0.7$. The solid lines and dashed lines correspond to the local Nusselt number along the upper and lower walls, respectively. The two sets of curves correspond to two values of the Reynolds number: $Re = 100$ and $Re = 500$.

An insight into the behavior of the local heat transfer coefficient can be obtained if attention is also focused on the corresponding flow and temperature fields in Figs. 3 and 7 for the same geometry. For the upper wall, the local heat transfer coefficient gradually decreases along the straight section upstream of the dimple, due to the slowing down of the flow. A local minimum is reached at a location corresponding to the junction between the straight wall and the dimple surface, where the flow is virtually stagnant. Then, the heat transfer coefficient increases rapidly along the upstream side of the dimple because of the core flow impingement. After reaching

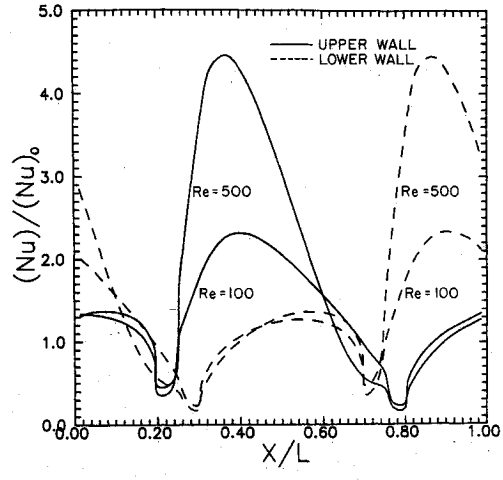

Fig. 14 Variation of local heat transfer for $Pr = 0.7$, $H/S = 0.32$, and $L/S = 1.875$.

a maximum value, the value decreases again along the downstream side of the dimple, where the heat transfer surface is in contact with either low speed flow (for $Re = 100$) or recirculating flow ($Re = 500$). A second minimum is reached at the junction of the dimple and the downstream straight wall, where the flow is stagnant. The heat transfer coefficient then rises along the straight wall as the fluid velocity adjacent to the wall increases in magnitude.

This pattern repeats itself cyclically and the variation of the heat transfer coefficient along the lower wall follows exactly the same pattern, except at different x/L locations. The values of the $Nu/\overline{Nu}_0$ ratios are, of course, higher for $Re = 500$, compared with the values for $Re = 100$.

Concluding Remarks

A control-volume finite-difference method based on general curvilinear coordinates has been developed to predict fully developed flow and heat transfer in streamwise-periodic geometries of complex shape. The method has been applied to predict velocity and temperature fields and overall quantities like friction factor and heat transfer coefficients for a parallel plate channel with dimples. The effect of parameters such as the Reynolds number, Prandtl number, dimple height to channel spacing ratio (H/S), and dimple spacing to channel spacing ratio (L/S) has been found to have an important bearing on the fluid flow and heat transfer performance. For large H/S and small L/S, the flowfield is characterized by large recirculation zones and significant flow distortion. Heat transfer augmentation compared to a parallel plate channel is as much as eight times for the range of parameters studied;

however, pressure drop can increase to as much as a factor of 18. The results indicate that channels with large H/S and small L/S ratios have larger heat transfer coefficients, but there may be no added benefit to increasing H/S to very large values. Details of the velocity field, temperature field, and the local heat transfer variation provide insights into the important physical phenomena.

Acknowledgments

The geometry studied in this work was suggested by Shyring Hu of McCord Heat Transfer Corporation. The assistance of J. A. Valenzuela and E. P. Childs of Creare Incorporated is also gratefully acknowledged.

References

[1]Patankar, S. V., Liu, C. H., and Sparrow, E. M., "Fully Developed Flow and Heat Transfer in Ducts Having Streamwise-Periodic Variations of Cross-Sectional Area," *ASME Journal of Heat Transfer,* Vol. 99, May 1977, pp. 180–186.

[2]O'Brien, J. E., and Sparrow, E. M., "Corrugated-Duct Heat Transfer, Pressure Drop and Flow Visualization," *ASME Journal of Heat Transfer,* Vol. 104, Aug. 1982, pp. 410–416.

[3]Kelkar, K. M., and Patankar, S. V., "Numerical Prediction of Flow and Heat Transfer in a Parallel Plate Channel with Staggered Fins," *ASME Journal of Heat Transfer,* Vol. 109, Feb. 1987, pp. 25–30.

[4]Karki, K. C., and Patankar, S. V., "A Calculation Procedure for Viscous, Incompressible Flows in Complex Geometries," *Numerical Heat Transfer,* Vol. 14, 1988, pp. 295–307.

[5]Asako, Y., and Faghri, M., "Finite-Volume Solutions for Laminar Flow and Heat Transfer in a Corrugated Duct," *ASME Journal of Heat Transfer,* Vol. 109, Aug. 1987, pp. 627–634.

[6]Garg, V. K., "Laminar Flow and Heat Transfer in a Periodically Converging-Diverging Channel," *International Journal for Numerical Methods in Fluids,* Vol. 8, 1988, pp. 579–597.

[7]Karki, K. C., "A Calculation Procedure for Viscous Flows at all Speeds in Complex Geometries," Ph.D. Thesis, Univ. of Minnesota, Minneapolis, MN, 1986.

[8]Patankar, S. V., *Numerical Heat Transfer and Fluid Flow,* Hemisphere, Washington, DC, 1980.

[9]Settari, A., and Aziz, K., "A Generalization of the Additive Correction Methods for the Iterative Solution of Matrix Equations," *SIAM Journal of Numerical Analysis,* Vol. 10, 1973, pp. 506–521.

[10]Thompson, J. F., Warsi, Z. U. A., and Mastin, C. W., *Numerical Grid Generation—Foundation and Applications,* North-Holland, NY, 1985.

[11]Goldstein, L., and Sparrow, E. M., "Heat Mass Transfer Characteristics for Flow in a Corrugated Wall Channel," *ASME Journal of Heat Transfer,* Vol. 99, May 1977, pp. 187–195.